Pergamon

Acta mater. Vol. 47, No. 1, pp. 77–88, 1999

Printed in Great Britain
PII: S1359-6454(98)00344-9
1359-6454/99 $19.00 + 0.00

DELAYED FRACTURE OF CERAMICS CAUSED BY STRESS-DEPENDENT SURFACE REACTIONS

H. H. YU and Z. SUO†

Mechanical and Aerospace Engineering Department, and Princeton Materials Institute, Princeton University, Princeton, NJ 08544, U.S.A.

(Received 21 July 1998; accepted in revised form 23 September 1998)

Abstract—Consider a ceramic in an environment, corroding gradually by a surface reaction. When in addition subject to a mechanical load, the ceramic loses mass preferentially at grain-boundary grooves where stress concentrates, so that atomistically sharp cracks may nucleate. Before becoming a crack, a groove maintains local equilibrium at its root; after, it loses local equilibrium. The crack further propagates by breaking atomic bonds, often assisted by environmental molecules. This paper models the groove-to-crack evolution. The groove changes shape to reduce the free energy due to the combined effects of surface tension, grain-boundary tension, elasticity, and chemical potential difference between the solid and the environment. At any point on the surface, the reaction rate is taken to be proportional to the free energy reduction per unit volume of mass loss. The ceramic body is modeled by a half plane bounded by a curve, whose shape is described by a conformal mapping of many terms, allowing the elastic field in the body to be solved analytically. A variational method leads to a set of ordinary differential equations to evolve the shape. The model predicts threshold loads, and the times required, for crack nucleation. © *1998 Acta Metallurgica Inc. Published by Elsevier Science Ltd. All rights reserved.*

1. INTRODUCTION

A brittle solid may withstand a static load for a long time and then, without warning, break suddenly. The smaller the load, the longer the delay time. The phenomenon is known as delayed fracture or static fatigue. A practically important question is whether a threshold stress exists—that is, whether there is a stress limit below which the solid can sustain the load indefinitely. Another question is how long the solid can sustain a stress above the threshold.

Orowan [1] attributed the phenomenon to an environmental effect on surface tension. According to Griffith, the strength S of a solid scales with its surface tension γ as $S \propto \gamma^{1/2}$. Certain molecules in air, adsorbing on the surfaces, reduce the surface tension. To affect fracture, the molecules must diffuse to a crack front, and assist in breaking atomic bonds. Both steps take time. Wiederhorn [2] reviewed evidence of glass weakened by water molecules. Within the framework of fracture mechanics, this theory has led to a procedure to predict lifetimes of engineering components [2, 3]. Cracks are assumed to pre-exist on the surface of a given engineering component, and grow slowly under a static stress. The time-to-fracture is the time required for one of the cracks to grow to a critical size. An upper bound of the initial crack size on the component surface is estimated by a proof test. To obtain a crack growth law, one cuts a sample of the same material with a long crack, loads it in a controlled environment, and measures the crack velocity as a function of stress intensity factor. The two pieces of information—the initial crack size and the crack growth law—are then used to predict a lower bound of the lifetime of the component.

This procedure has been successfully applied to components with relatively large initial crack sizes and short lifetimes. How to apply the procedure to components like microelectronic chips is uncertain. The feature size on a chip is about 1 μm. The initial flaw is ill-defined, and the total crack growth should be less than the feature size. Suppose that 10 years of lifetime is required; the allowed crack velocity should be lower than 10^{-14} m/s. Direct measurement of such low crack velocities is extremely difficult. One is then forced to do accelerated tests, or find a way to determine the threshold condition. To extrapolate the data to predict lifetime, one must understand what happens at low crack velocities or near the threshold condition.

That atomistically sharp cracks pre-exist in materials has always been a vexing assumption. Hillig and Charles [4] and others [5–15] have considered a different theory of delayed fracture. Initial flaws can be blunt. A solid loses mass to its environment by a surface reaction; the rate of the reaction depends on local stress. Because the stress along a flaw surface is non-uniform, the reaction may proceed faster at the flaw root than elsewhere, gradually changing the flaw into a sharp crack. Alternatively, at elev-

†To whom all correspondence should be addressed.

ated temperatures, a flaw can change shape by mass transport due to surface diffusion, evaporation–condensation, etc. Newcomb and Tressler [16] observed fracture of sapphire fibers at high temperatures. Micron-sized pores were left inside the fibers in a manufacturing process. When the fibers were loaded in tension, delayed fracture often originated from these internal pores. The experimental observations were interpreted as follows [13]. A pore may change shape by surface diffusion. Surface tension tends to keep the pore rounded, but the applied stress tends to change the pore shape to form a sharp crack front. Consequently, the model predicts a threshold condition: the pore reaches an equilibrium shape close to an ellipse when the applied stress is small, but forms a crack front when the applied stress is large. Most models in the literature relied on elasticity solutions for elliptic or ellipsoidal holes. However, before forming a crack front, a pore becomes eye-shaped, localizing the shape change and shortening the diffusion length. Recent models [14, 15] allowed such non-elliptic shapes, better estimating the crack nucleation time.

The two theories of delayed fracture do not oppose each other; rather, they complement. In the above example, if the applied stress exceeds the threshold, a fiber may spend its lifetime in two stages [14]. First, a pore pre-existing in the fiber changes shape by surface diffusion to form a crack front. Then the crack extends by a slow bond-breaking process to attain the critical size for fast fracture. The two stages involve different rate processes. The total lifetime can be dominated by either crack nucleation or crack growth, depending on pore size, stress level, temperature, etc.

Asaro and Tiller [17] and others [18–21] showed that even a flat surface under a stress is unstable, and can evolve to a wavy shape by surface diffusion. Chiu and Gao [22], and Yang and Srolovitz [23] further showed that the wavy surface can evolve to form a sharp crack front. The process was observed by Jesson *et al.* [24] on a surface of a strained epitaxial film. Thus, a stress-concentrating flaw is unnecessary for crack nucleation. Furthermore, there is no threshold condition for crack nucleation, that is a crack can nucleate at arbitrarily small stress. The practical significance of the findings has been understood in terms of time. The system has a natural length scale $L = \gamma E/\sigma^2$, where γ is the surface tension, E Young's modulus, and σ the applied stress. When the dominant mass transport mechanism is surface diffusion, with mass mobility M, the crack nucleation time-scales as $t_N \propto L^4/M\gamma$. If cracks take too much time to nucleate, because either the stress or the temperature is low, the process should be ignored so far as lifetime is concerned.

A perfectly flat surface is an idealization. Most real surfaces have flaws due to abrasion or machining. For polycrystalline materials, grain boundaries cause surfaces to form grooves. In integrated microstructures, sharp material discontinuities such as corners are present. These features all concentrate stress. This paper studies cracks nucleating from the grooves on polycrystalline surfaces. At high temperatures, when a ceramic is under a tensile load parallel to the surface, matter on the surface can diffuse into and along a grain boundary. This process can lead to a notch growing along the grain boundary under certain conditions [25, 26]. Mass inserted into the grain boundary alleviates the stress concentration so that such a notch is usually not atomistically sharp. In this paper, following Suo and Yu [27], we consider another situation: the grain boundary does not transport mass, but the surface changes shape by evaporation–condensation or a chemical reaction. This process may dominate at relatively low temperatures and in corrosive environments. Two types of behaviors are expected. If the applied stress is small, the grooves approach a steady shape, and the ceramic loses mass evenly on the surface. If the applied stress is large, the grooves sharpen into crack fronts, and the cracks subsequently grow by decohesion.

A main difficulty in analyzing the model is to determine the elastic field in a body with a curved surface. Following Chiu and Gao [22], who solved the elastic field in a plane bounded by a cycloid, we modeled the evolving polycrystalline surface by a family of cycloids [27]. The family had two degrees of freedom: one described gross mass loss, and the other the surface shape. This low-dimensional model predicted the trends of threshold stress and nucleation time. The model, however, did not contain enough degrees of freedom to give quantitatively reliable results. In particular, the geometry of the cycloid dictated that a crack should form when the groove depth reached $1/\pi$ times the grain size. In reality, when the applied stress is large, the grooves are expected to be more localized, and the groove depth can be much smaller when the crack forms; the localization significantly shortens the crack nucleation time.

The object of the present paper is to use more degrees of freedom to model localized grooving. We first outline the physical aspects of the model, and then use a family of curves to describe the boundary of the ceramic body. The elastic field is solved analytically in Appendix B. In Appendix A, we discuss the local equilibrium and the loss of it at a groove root. A variational approach is used to construct a dynamical system to evolve grooves. The paper finally presents simulation results.

2. PHYSICAL DISCRIPTION OF THE MODEL

Figure 1 illustrates the two-dimensional model. Represent a ceramic body by a half plane and its surface by a curve. All grains have the same size λ. The surface tension γ_S and the grain-boundary ten-

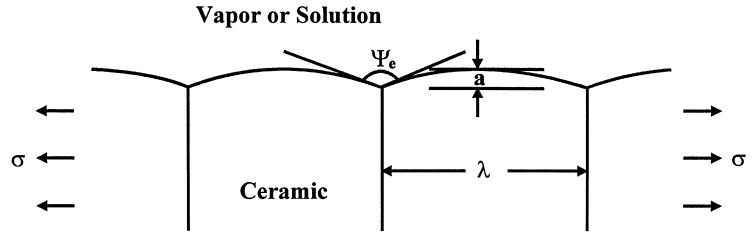

Fig. 1. A ceramic in a corrosive environment, subject to a stress parallel to the surface.

sion γ_B are taken to be isotropic. They are the values obtained after the ceramic is exposed to the environment (e.g. a vapor or a solution) for a prolonged time. Within the environment, the molecular mobility is so large that the chemical potential is uniform. The solid and the environment, however, are not in equilibrium with each other: they exchange mass by dissolution or precipitation. Denote g as the free energy increase per unit volume of solid deposited on a flat, stress-free surface. We assume that the solid is immersed in such a large environment that the chemical potential of the environment changes negligibly during the reaction. Thus, g is a constant in this model. The solid is subject to a remote stress σ in the horizontal direction, and remains elastic—that is no dislocation or diffusional creep occurs to alleviate the stress concentration at the groove roots. Furthermore, if condensation or precipitation occurs, mass attaches to the solid coherently, introducing no dislocations or pores.

As the surface reaction proceeds, the solid–environment, as a system, reduces its free energy. The displacement at the loading point is held fixed so that the loading device does no work to the ceramic as the surface evolves. The total free energy, G, consists of the surface energy U_S, the grain-boundary energy U_B, the chemical energy U_C, and the elastic energy U_E. Thus,

$$G = U_S + U_B + U_C + U_E \tag{1}$$

In our model, the energy is given per grain per unit thickness, to be calculated in the next section.

Three dimensionless groups measure the relative significance of the various energetic forces:

$$\Gamma = \frac{\gamma_B}{\gamma_S}, \Lambda = \frac{\sigma^2 \lambda}{E\gamma_S}, \chi = \frac{g\lambda}{\gamma_S} \tag{2}$$

Their qualitative significance is readily understood. When $\Gamma > 2$, the free energy reduces as two free surfaces replace one grain boundary, so that a triple junction loses local equilibrium: atomic bonds break spontaneously along the grain boundary even under no applied stress. Our model will be restricted to $0 \le \Gamma \le 2$. Local equilibrium dictates that the dihedral angle Ψ_e in Fig. 1 be given by $\cos(\Psi_e/2) = \gamma_B/2\gamma_S$.

The normalized load can take any value $\Lambda \ge 0$, and tends to destabilize grooves. As shown in Appendix A, under stress, as the surface changes shape, the groove becomes more localized, but the equilibrium dihedral angle is maintained. The stress field at the groove root is singular. So is the local curvature. Before the groove becomes a crack, the singularity is so weak that the elastic field does not give an energetic force to drive the motion of the triple junction. After a sharp crack is formed, the two surfaces becomes parallel at the triple junction, the local equilibrium is lost; the elastic energy, as well as the surface and the grain-boundary tension, contributes to the driving force on the triple junction. Thus, both the groove and the crack cause a singular stress field within the linear elasticity theory; the exponents of the singularity are different, so that the groove maintains local equilibrium, but the crack does not.

The normalized chemical free energy, χ, may take any value. When $\chi > 0$, a solid with a flat, stress-free surface has a higher free energy than the environment, and the solid dissolves. When $\chi < 0$, a solid with a flat, stress-free surface has a lower free energy than the environment, and the solid precipitates. A solid surface, if curved or under stress, dissolves or precipitates even when $\chi = 0$, depending on the total free energy G. Although the chemical free energy χ can take very large values, by itself it can never drive a groove into a crack. Stress concentration is a prerequisite for crack formation. In fact, our simulation results will show that χ makes little contribution to the crack nucleation process.

We now consider the kinetic process, following a variational approach described by Suo [28]. Let $\mathscr{p}$ be the free energy reduction associated with a unit volume of mass attached coherently to the solid surface. When a surface element ds moves by a distance δr_n, the free energy reduces by $\mathscr{p}\delta r_n ds$. Consequently, associated with the entire surface motion, the total free energy variation, δG, is given by

$$\int \mathscr{p}\delta r_n \mathrm{d}s = -\delta \mathscr{G} \tag{3}$$

The integral is over the surface per grain. Because δr_n is an arbitrary virtual motion, this relation defines the driving force for the surface reaction, $\mathscr{p}$,

at every point on the surface. The actual normal velocity of the surface is a function of the driving force. For simplicity, we adopt a linear kinetic law:

$$v_n = m\not{F} \tag{4}$$

where m is the specific reaction rate. A special case of a more general law introduced by Hillig and Charles [4], this linear kinetic law is valid when the driving force is small compared to the average thermal energy. Because little is known quantitatively of the general law, this paper is restricted to the linear law. Eliminating $\not{F}$ from equations (3) and (4), we obtain that

$$\int \frac{v_n \delta r_n}{m} \mathrm{d}s = -\delta G \tag{5}$$

This is the *weak statement*, which will be used in the next section to evolve the ceramic surface. Temperature enters the model through the specific reaction rate m.

This paper assumes that the grain-boundary grooves are the only geometric features on the solid surface. Two points need be clarified here. First, the ceramic is assumed to be well annealed: other than the grain-boundary grooves, no imperfection such as cracks or holes exist on the surface. With such a perfect surface, a crack may still nucleate on a grain surface, away from the grain boundaries, as shown in Fig. 2(a). Such a crack, however, should take a longer time to nucleate than those along the groove roots. Thus we focus on cracks nucleating from the groove roots. Second, under a small applied stress, the periodic grooves can be unstable against a perturbation of a wavelength larger than the grain size [Fig. 2(b)]. Here we tentatively assume that such cracks take a very long time to nucleate, and will treat them elsewhere.

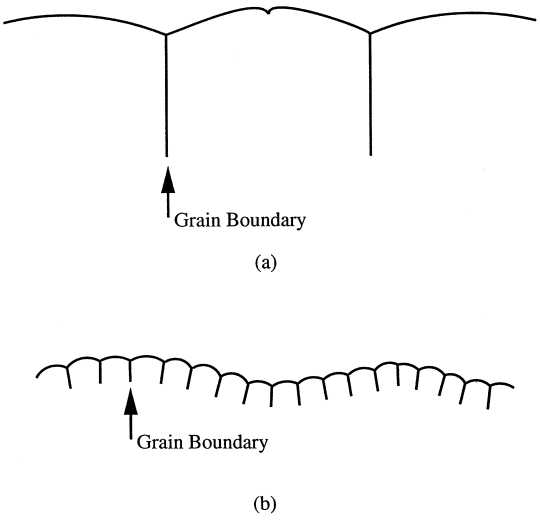

Fig. 2. (a) Solid forms a crack away from the grain boundary. (b) Solid has a surface perturbation with wavelength larger than the grain size.

3. EVOLUTION EQUATIONS

3.1. Shape of the ceramic boundary

We describe the boundary of the ceramic by a family of curves:

$$kx = \theta + \alpha_1 \sin\theta + \ldots + \alpha_n \sin n\theta \tag{6a}$$

$$ky = \alpha_0 + \alpha_1 \cos\theta + \ldots + \alpha_n \cos n\theta \tag{6b}$$

Here $k = 2\pi/\lambda$, and the α values are dimensionless real numbers. As θ varies, $-\infty < \theta < +\infty$, the point (x,y) traces the boundary. Chiu and Gao [22] used one term (the α_1 term) in their work. The term α_0 is added to represent uniform mass gain or loss. To adequately describe highly localized grooves, this paper extends the family: the more terms, the more kinds of curves the family includes. As the coefficients $\alpha_0,\alpha_1,\ldots,\alpha_n$ evolve with time, the surface changes its shape. When $\alpha_0 = \alpha_1 = \ldots = \alpha_n = 0$, the ceramic surface is flat. This is taken to be the energy reference state. When the crack tips form at the groove roots ($\theta = \pm\pi, \pm 3\pi, \ldots$), the surface normal vector becomes horizontal, so that

$$1 - \alpha_1 + \ldots + (-1)^n n\alpha_n = 0 \tag{7}$$

This condition ends our calculation. Here we simulate the crack formation process, not the subsequent decohesion process.

As explained in Appendix B, this family of curves is given by a conformal mapping, which allows the elastic field in the half plane bounded by such curves to be solved analytically. The curves are smooth during the entire simulation before cracks form. On the other hand, at the root of a groove, the surface is not smooth, but forms an equilibrium dihedral angle Ψ_e. Furthermore, the elastic stress field at such a groove root is singular. Consequently, our simulation based on the smooth curves does badly for the geometry and stress field at the groove root. There is nothing unusual about this situation, however. As shown in Appendix A, the local equilibrium is implied by the weak statement as a natural boundary condition. In approximation methods based on weak statements, such as finite element analysis for stress field, natural boundary conditions are seldom satisfied exactly; rather, they are satisfied in some average sense. As will be shown below, our simulation results agree well with the known exact solutions, all the way to points very close to the groove root. The more terms in equations (6a) and (b) we use, the better the shape.

The curve element is

$$\mathrm{d}s = \sqrt{\mathrm{d}x^2 + \mathrm{d}y^2}$$

where

$$k\mathrm{d}x = \left(1 + \alpha_1 \cos\theta + \ldots + n\alpha_n \cos n\theta\right)\mathrm{d}\theta \tag{8a}$$

$$k\mathrm{d}y = \left(-\alpha_1 \sin\theta - \ldots - n\alpha_n \sin n\theta\right)\mathrm{d}\theta \qquad (8b)$$

Consequently, all the integrals per grain surface are carried with respect to θ, in the interval $(-\pi,\pi)$.

3.2. Energy calculation

Appendix B solves the elastic field in a half plane bounded by a curve represented by equations (6a) and (b). With the aid of Fig. 3, note that U_E is the difference of the elastic energy stored in the current body and in the reference body. Both bodies are subject to the horizontal stress σ. Figure 3 also shows an imaginary body whose shape is identical to the current body, but whose body is under a uniform stress σ. To maintain this stress field in the imaginary body, a distribution of surface stress σn_x must be applied, where n_x is the horizontal component of the surface normal vector. The additional elastic displacement of the current body relative to the imaginary body is

$$u_x = -\frac{2\sigma}{kE}\left(c_1 \sin\theta + \ldots + c_n \sin n\theta\right) \qquad (9)$$

The coefficients c are dimensionless functions of α, as given in Appendix B. The elastic energy difference between the current body and the imaginary body is the work done in removing the surface stress, $-(1/2)\int u_x \sigma n_x \mathrm{d}s$. The elastic energy difference between the imaginary body and the reference body is the energy density $\sigma^2/2E$ times the area $\int y\mathrm{d}x$. The sum of the two differences is the excess elastic energy stored in the current body relative to the reference body. Integrating, we find that

$$U_E = \frac{\pi\sigma^2}{k^2E}\left[\frac{1}{2}\left(2\alpha_0 + \alpha_1^2 + \ldots + n\alpha_n^2\right) - \left(c_1\alpha_1 + \ldots + nc_n\alpha_n\right)\right] \qquad (10)$$

The excess energy per grain boundary is the grain-boundary tension times the height of the grain boundary,

$$U_B = \frac{\gamma_B}{k}\left[\alpha_0 - \alpha_1 + \ldots + (-1)^n\alpha_n\right] \qquad (11)$$

The excess surface energy is

$$U_S = \gamma_S \int \mathrm{d}s - \gamma_S\lambda \qquad (12)$$

This integral is carried out numerically. The excess chemical energy is g times the area $\int y\mathrm{d}x$, so that

$$U_C = \frac{\pi g}{k^2}\left(2\alpha_0 + \alpha_1^2 + 2\alpha_2^2 + \ldots + n\alpha_n^2\right) \qquad (13)$$

3.3. Virtual motion

When a small amount of mass is added to or removed from the ceramic surface, it changes the surface shape and position slightly. Describe the small variation of the surface by a set of variations $\delta\alpha_0,\delta\alpha_1,\ldots,\delta\alpha_n$. In the above we have calculated the free energy as a function of curve shape, i.e. $G(\alpha_0,\alpha_1,\ldots,\alpha_n)$. The energy variation associated with the motion is written as

$$\delta G = -f_0\delta\alpha_0 - f_1\delta\alpha_1 - \ldots - f_n\delta\alpha_n \qquad (14)$$

The expressions of the generalized forces $f_0,f_1,\ldots,f_n$ are given in Appendix C. They are functions of $\alpha_0,\alpha_1,\ldots,\alpha_n$.

Associated with the virtual change, a point (x,y) on the surface moves by a small distance, $(\delta x,\delta y)$, given by

$$k\delta x = \sin\theta\delta\alpha_1 + \ldots + \sin n\theta\delta\alpha_n \qquad (15a)$$

$$k\delta y = \delta\alpha_0 + \cos\theta\delta\alpha_1 + \ldots + \cos n\theta\delta\alpha_n \qquad (15b)$$

The components of the unit normal vector are $n_x = -\partial y/\partial s$ and $n_y = \partial x/\partial s$. An element $\mathrm{d}s$ moves in the normal direction by a small distance $\delta r_n = n_x\delta x + n_y\delta y$, given by

$$k\delta r_n = A_0\delta\alpha_0 + A_1\delta\alpha_1 + \ldots + A_n\delta\alpha_n \qquad (16)$$

with

$$A_p = \left[\cos p\theta + \alpha_1\cos(p-1)\theta + \ldots + n\alpha_n\cos(p-n)\theta\right]\frac{\partial\theta}{k\partial s} \qquad (17)$$

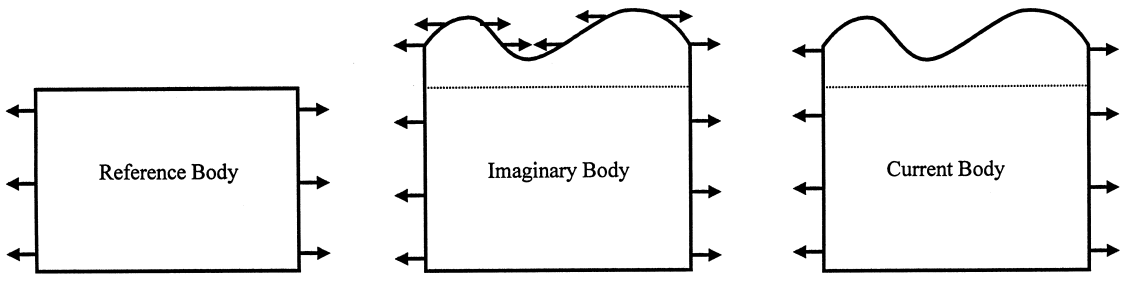

Fig. 3. Bodies used in calculating excess elastic energy.

The normal velocity of the surface, v_n, is written as

$$kv_n = A_0\dot{\alpha}_0 + A_1\dot{\alpha}_1 + \ldots + A_n\dot{\alpha}_n \qquad (18)$$

The superimposed dots denote time derivatives.

Inserting equations (14), (16) and (18) into the weak statement given by equation (5), we obtain that

$$\sum_{q=0}^{n} H_{pq}\dot{\alpha}_q = f_p \qquad (19)$$

with the generalized viscosity being

$$H_{pq} = \frac{1}{mk^2}\int A_p A_q \mathrm{d}s \qquad (20)$$

Note that equation (19) is a set of nonlinear ordinary differential equations. They are solved numerically to evolve the coefficients $\alpha_0,\alpha_1,\ldots,\alpha_n$, and thereby the curve.

4. EVOLVING GROOVES

4.1. Steady surface motion in the absence of stress

In the absence of the stress, evolution is driven by the surface tension, the grain-boundary tension, and the chemical energy. The surface always approaches an invariant shape moving steadily as the solid dissolves to or precipitates from the environment. The steady shape of the surface has been solved analytically [28], given by

$$\frac{x}{\lambda} = \frac{1}{c\chi}\begin{cases} \Phi - \dfrac{1}{\sqrt{1-c^2}}\tan^{-1}\left(\dfrac{\sqrt{1-c^2}\,\sin\Phi}{c+\cos\Phi}\right) & c^2<1 \\ \Phi - \dfrac{1}{\sqrt{c^2-1}}\tanh^{-1}\left(\dfrac{\sqrt{c^2-1}\,\sin\Phi}{c+\cos\Phi}\right) & c^2>1 \end{cases} \qquad (21a)$$

$$\frac{y}{\lambda} = -\frac{1}{c\chi}\ln|c\cos\Phi + 1| \qquad (21b)$$

The parameter c relates to the steady state velocity as $c = v/mg$. As the tangent angle Φ varies from $-(\pi-\Psi_e)/2$ at $x = \lambda/2$ to $(\pi-\Psi_e)/2$ at $x = -\lambda/2$, equations (21a) and (b) traces the grain surface. For a given pair of χ and Ψ_e, c is determined by using equation (21a), with $x = \lambda/2$ and $\Phi = -(\pi-\Psi_e)/2$.

Figure 4 compares the exact surface shapes (solid lines) with the approximate shapes (open circles) obtained by using the weak statement. The shapes agree well even for large values of χ. When $\chi = -50$, the solid gains mass, and the groove is relatively localized. When $\chi = 100$, the solid loses mass, and the surface near the grain boundary is almost straight. Although the dihedral angle cannot be represented by the numerical simulation, the surface shapes are well approximated all the way to points very close to the groove root. In the absence of stress, the groove root always maintains local equilibrium, and cannot evolve into a sharp crack.

4.2. Two behaviors: approaching steady state or forming crack

Figure 5 shows the time sequences of the surfaces under three applied stress levels. The initial surface is taken to be flat. At a small stress [$\Lambda = 1$, Fig. 5(a)], the surface approaches a steady shape, the body loses mass evenly over the entire surface, and no crack is formed. At a large stress [$\Lambda = 3$, Fig. 5(b)], the surface never reaches a steady shape, the body loses mass preferentially at the groove root, and a crack forms on the surface. At an even larger stress [$\Lambda = 20$, Fig. 5(c)], the shape change is more localized, and the crack forms at a smaller groove depth and in shorter time.

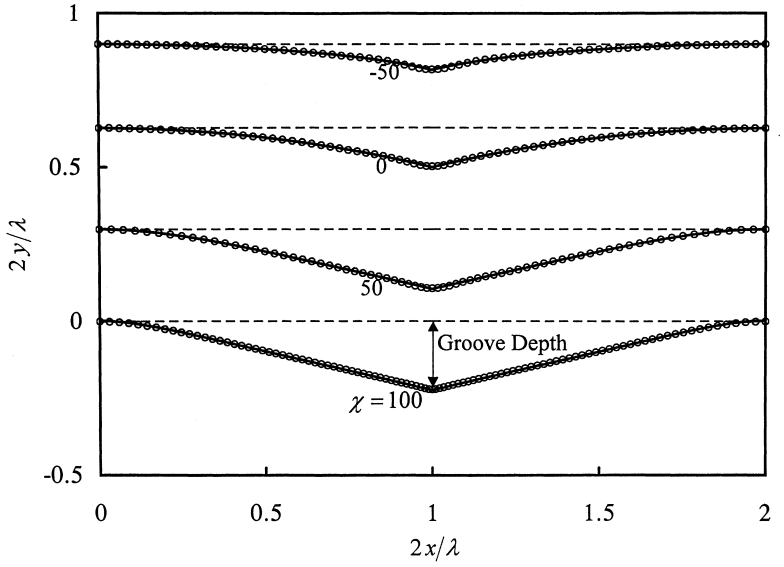

Fig. 4. A comparison of the exact and approximate steady state groove shapes. No stress is applied. $\Gamma = 0.5$.

Figure 6 plots the groove depths as functions of time in logarithm scale. When the applied stress is small, the groove approaches a steady depth. When the applied stress is large, the crack nucleation time is short and the crack depth is small. As a supercritical groove sharpens, the grooving velocity approaches infinity. This is because once the crack front forms, the triple junction loses local equilibrium, and subsequent crack extension is not limited by surface mass exchange. Other processes should be invoked to limit the crack velocity, such as stress-wave propagation or diffusion of environmental molecules to the crack front to lower the surface tension. This paper does not study the decohesion process after crack nucleation.

As discussed above, when a ceramic is subject to a stress, the surface either approaches a steady shape or forms cracks. There exists a threshold stress for crack nucleation. Figure 7 plots the normalized threshold stress as a function of χ and Γ. Under a condition below a corresponding line, a polycrystalline surface approaches a steady shape; above it, the surface nucleates cracks. The threshold Λ increases when the solid gains mass (large negative χ), and almost remains constant when the solid loses mass (positive χ). In the latter case, the threshold stress is close to the estimation [27]:

$$\left(\frac{\sigma^2\lambda}{E\gamma_S}\right)_{th} = 4 - 2\frac{\gamma_B}{\gamma_S} \tag{22}$$

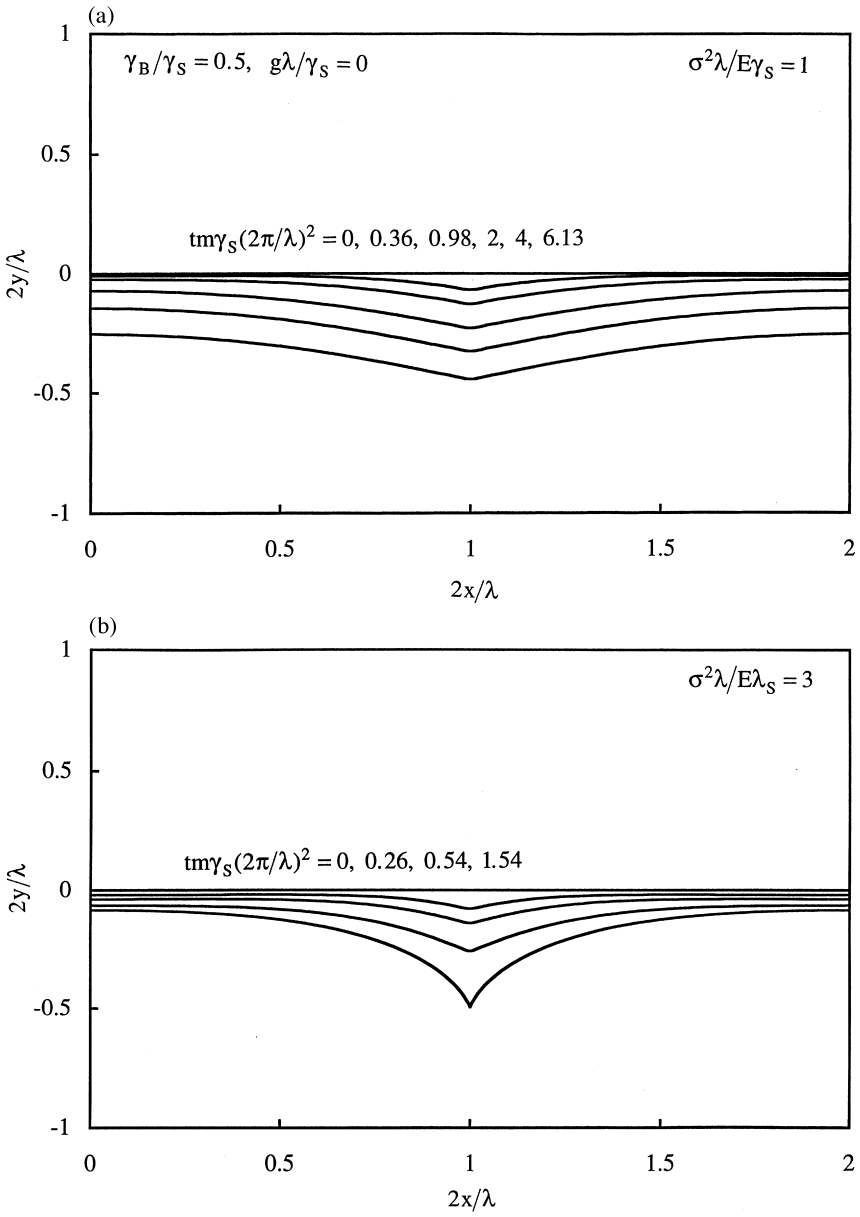

Fig. 5. Time sequences of surface shapes: (a) $\Lambda = 1$; (b) $\Lambda = 3$; and (c) $\Lambda = 20$.

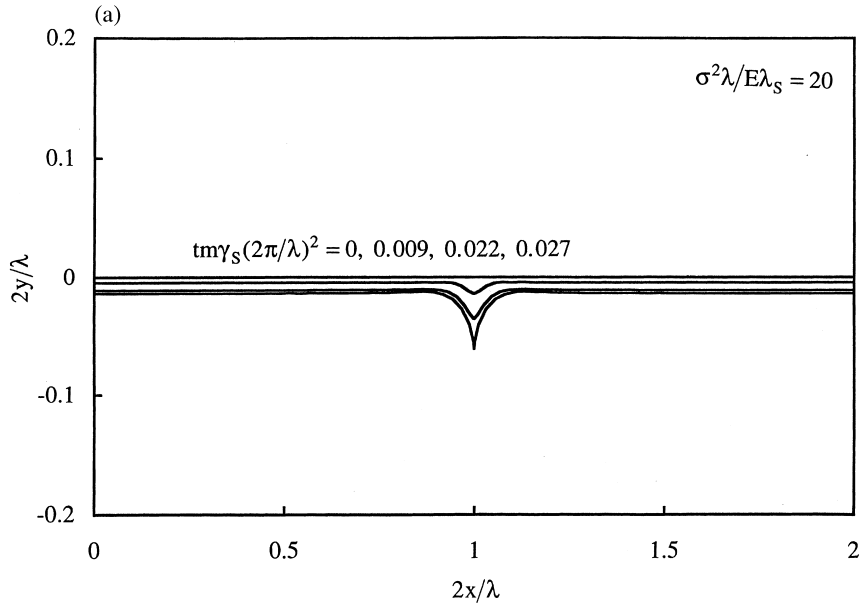

Fig. 5(c)

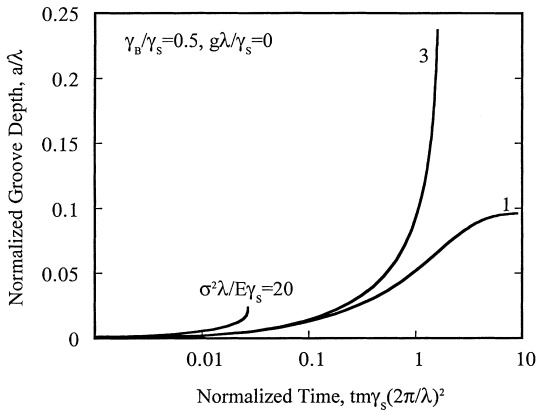

Fig. 6. Groove depths as functions of time.

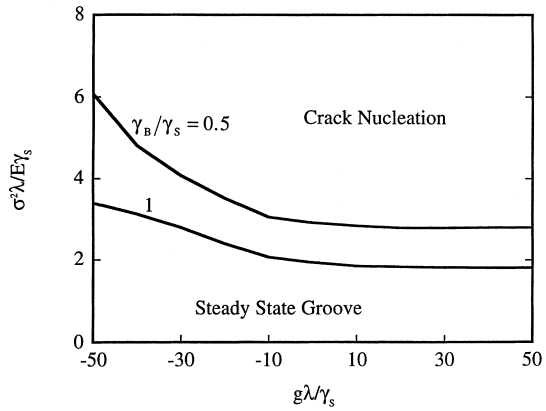

Fig. 7. Threshold condition.

In this case, the chemical free energy χ plays a negligible role on the value of threshold stress.

The existence of threshold is partly due to a constraint of our model. We have assumed that the wavelength of the curve coincides with the grain size. If, as pointed out earlier, the wavelength is allowed to exceed the grain size [Fig. 2(b)], some grains losing more mass than others, cracks may nucleate at stresses lower than the threshold given above, over a long time-scale. We will explore this behavior elsewhere.

4.3. Crack nucleation time and crack size

Above the threshold condition, an initially flat polycrystalline surface nucleates a crack in a finite time. In the two-degrees-of-freedom model, the shape of the curve is constrained such that the crack always forms at the groove depth $a = \lambda/\pi$ [27]. Consequently, the model cannot predict the crack size accurately when a groove localizes within

Table 1. The effects of the degrees of freedom

n	τ_N	a/λ
2	1.33	0.318
4	0.47	0.145
8	0.25	0.095
12	0.20	0.079
16	0.19	0.074
20	0.186	0.072
24	0.1841	0.0708
28	0.1839	0.0703

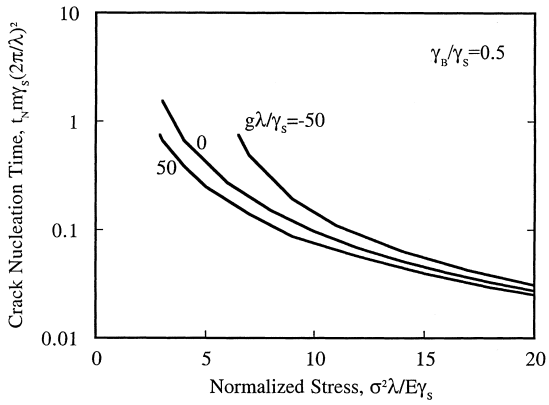

Fig. 8. The time needed for an initially flat polycrystalline surface to nucleate crack fronts.

a length scale much smaller than the grain size. Neither can it simulate the steady state with normalized groove depth larger than λ/π. As mentioned before, the more the degrees of freedom, the more flexibly the surface can change its shape. Table 1 shows the effect of the degrees of freedom on the crack nucleation time and crack size when the crack just forms for the supercritical case $\Gamma = 0.5$, $\chi = 50$ and $\Lambda = 6$. The nucleation time calculated from the two-degrees-of-freedom model [27] is about one order of magnitude longer than the value from the 28-degrees-of-freedom model, so is the crack size when the crack just forms. In this paper, we have increased the degrees of freedom until the results are insensitive to the change.

The nucleation time takes the form

$$t_N = \frac{\lambda^2}{(2\pi)^2 m\gamma_S}\tau(\Gamma,\chi,\Lambda) \tag{23}$$

where $\tau(\Gamma,\chi,\Lambda)$ is a dimensionless function. Here we use the grain size λ to scale the time, rather than the length L given in Section 1. The latter depends on the applied stress, which complicates the interpretation in the present situation. Figure 8 plots the nucleation time as a function of load. These curves resemble the lifetime–stress plots in the experimental literature on delayed fracture. A solid losing mass forms crack faster than a solid gaining mass. However, when the applied stress is far beyond the threshold, the chemical energy parameter χ affects the nucleation time negligibly. Figure 9 plots the crack size (when it just forms) as a function of normalized load. When the applied stress is large, the crack can form at a very small groove depth. The value of χ has little effect on the crack size.

5. CONCLUDING REMARKS

When a solid is under a static load in a corrosive environment, delayed fracture can proceed by first nucleating cracks, and then extending the cracks. The two stages involve different kinetic processes: the former, surface reactions; and the latter, environment-assisted bond breaking. Either process can dominate the time-to-fracture, depending on experimental conditions. A better understanding of the crack nucleation process is expected to be important to lifetime prediction for integrated microstructures, where feature size is small and desired lifetime is long. This paper presents a model of the crack nucleation process on a ceramic surface by stress-dependent surface reaction. The ceramic surface changes its shape by mass exchange with environment, but the bulk deforms elastically. When the applied stress is large, grain-boundary grooves sharpen, leading to cracks. Elastic field in a half plane with a curved boundary is solved analytically. The curve is described with many degrees of freedom to simulate localized grooving. Numerical results include the time sequences of groove shapes, the threshold condition for crack nucleation, and the time required for a surface to form cracks. Further calculations with wavelengths longer than the grain size are required to clarify whether a true

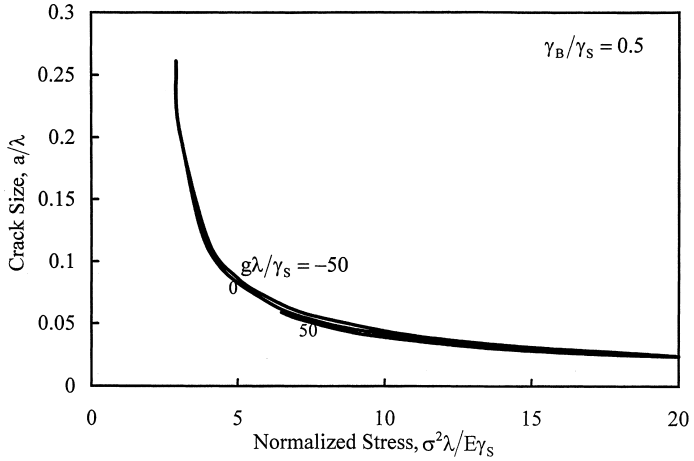

Fig. 9. The crack size when it just forms.

threshold exists. The large surface shape change due to the applied stress should be readily detected experimentally. It is hoped that experiments will soon succeed in ascertaining the significance of the process in real materials.

Acknowledgements—This work was supported by the National Science Foundation through grant MSS-9202165, and by The Institute for Materials Research and Engineering, Singapore.

REFERENCES

1. Orowan, E., *Nature*, 1944, **154**, 341.
2. Wiederhorn, S. M., *J. Non-Cryst. Solids*, 1975, **19**, 169.
3. Evans, A. G. and Wiederhorn, S. M., *Int. J. Fract.*, 1974, **10**, 379.
4. Hillig, W. B. and Charles, R. J., in *High-Strength Materials*, ed. V. F. Zackay. Wiley, New York, 1964, pp. 682–705.
5. Stevens, R. N. and Dutton, R., *Mater. Sci. Engng*, 1971, **8**, 220.
6. McCartney, L. N., *Acta metall.*, 1977, **25**, 221.
7. Heald, P. T. and Speight, M. V., *Mater. Sci. Engng*, 1977, **29**, 271.
8. Chuang, T. J. and Fuller, E. R., *J. Am. Ceram. Soc.*, 1992, **75**, 540.
9. Yacobson, B. I., *J. chem. Phys.*, 1993, **99**, 6923.
10. Gao, H., *Q. J. Mech. appl. Math.*, 1992, **45**, 149.
11. Gao, H., *Proc. R. Soc. A*, 1995, **448**, 465.
12. Suo, Z. and Wang, W., *J. appl. Phys.*, 1994, **76**, 3410.
13. Sun, B., Suo, Z. and Evans, A. G., *J. Mech. Phys. Solids*, 1994, **42**, 1653.
14. Wang, W. Q. and Suo, Z., *J. Mech. Phys. Solids*, 1997, **45**, 709.
15. Xia, L., Bower, A. F., Suo, Z. and Shih, C. F., *J. Mech. Phys. Solids*, 1997, **45**, 1473.
16. Newcomb, S. A. and Tressler, R. E., *J. Am. Ceram. Soc.*, 1993, **76**, 2505.
17. Asaro, R. J. and Tiller, W. A., *Metall. Trans.*, 1972, **3**, 1789.
18. Grinfeld, M., *Soviet Phys. Dokl.*, 1986, **31**, 831.
19. Srolovitz, D. J., *Acta metall.*, 1989, **37**, 621.
20. Spencer, B. J., Voorhees, P. W. and Davis, S. H., *Phys. Rev. Lett.*, 1991, **67**, 3696.
21. Freund, L. B. and Jonsdottir, F., *J. Mech. Phys. Solids*, 1993, **41**, 1245.
22. Chiu, C. H. and Gao, H., *Int. J. Solids Struct.*, 1993, **30**, 2981.
23. Yang, W. H. and Srolovitz, D. J., *Phys. Rev. Lett.*, 1993, **71**, 1593.
24. Jesson, D. E., Pennycook, S. J., Baribeau, J.-M. and Houghton, D. C., *Phys. Rev. Lett.*, 1993, **71**, 1744.
25. Chuang, T. J. and Rice, J. R., *Acta metall.*, 1973, **21**, 1625.
26. Chuang, T. J., *J. Am. Ceram. Soc.*, 1982, **65**, 93.
27. Suo, Z. and Yu, H., *Acta mater.*, 1997, **45**, 2235.
28. Suo, Z., *Adv. appl. Mech.*, 1997, **33**, 194.
29. Muskhelishvili, *Some Basic Problems of the Mathematical Theory of Elasticity*. P. Noordhoff Ltd., Groningen, The Netherlands, 1953.

APPENDIX A

Dihedral angle, local equilibrium, and crack formation

Before a crack forms, the surfaces at a groove root make an angle Ψ. When the surface undergoes a virtual motion δr_n and the groove root deepens by δa, the free energy varies by

$$\delta G = \int (W + g + \gamma_S \kappa)\delta r_n \mathrm{d}s + \left(2\gamma_S \cos\frac{\Psi}{2} - \gamma_B\right)\delta a \quad \text{(A1)}$$

where W is the elastic energy per unit volume, and κ is the surface curvature. The quantity in the first term is the driving force for surface motion; the second, for groove root motion. Because the virtual motions δr_n and δa are arbitrary, a comparison to the weak statement of equation (5) shows that the surface driving force relates to the surface velocity:

$$v_n = -m(W + g + \gamma_S \kappa) \quad \text{(A2)}$$

and the groove driving force vanishes:

$$\cos\left(\frac{\Psi_e}{2}\right) = \frac{\gamma_B}{2\gamma_S} \quad \text{(A3)}$$

Thus, the equilibrium dihedral angle given in equation (A3) is the consequence of local equilibrium. It comes out as a natural boundary condition of the weak statement, which implicitly assumes that the kinetic process at the grooving root is infinitely fast.

Because the dihedral angle Ψ_e is preserved, the stress field is singular at the groove root. Let R be a small distance from the groove root. The stress field in the solid scales as $R^{-\mu}$, where $0 < \mu < 1/2$. Consequently, near the root $W \propto R^{-2\mu}$. In equation (A2), because g is a constant, to maintain a finite surface velocity, the curvature must also be singular. The stress singularity is weak so that the integral in equation (A1) is finite for any reasonable δr_n. Consequently, the weak statement of equation (5) is well posed.

When a sharp crack forms, the surfaces at the root become parallel, the stress field becomes $R^{1/2}$ singular, and the energy variation becomes

$$\delta G = \int (W + g + \gamma_S \kappa)\delta r_n \mathrm{d}s + (2\gamma_S - \gamma_B - \mathscr{G})\delta a \quad \text{(A4)}$$

where $\mathscr{G}$ is the elastic energy release rate. If no mass is added to or removed from the crack surfaces, the integral in equation (A4) extends over only the surface away from the crack. Local equilibrium now requires that

$$\mathscr{G} = 2\gamma_S - \gamma_B \quad \text{(A5)}$$

Because $\mathscr{G}$ depends on the crack length, equation (A5) can only be satisfied by one crack length. When the crack front loses local equilibrium, the weak statement of equation (5) is ill-posed. A kinetic law for the decohesion process should be specified to limit the crack velocity. In our simulation, we stop the calculation when the crack emerges.

APPENDIX B

Elastic field in a half plane with a curved boundary

We use the method of complex variables to solve the elastic field. In Fig. 1 the physical plane is (x,y). Define a complex variable $z = x + \mathrm{i}y$, where $\mathrm{i} = \sqrt{-1}$. Introduce another plane (θ,η) and denote $\zeta = \theta + \mathrm{i}\eta$. The function

$$kz = \zeta + \mathrm{i}(\alpha_0 + \alpha_1 \mathrm{e}^{-\mathrm{i}\zeta} + \ldots + \alpha_n \mathrm{e}^{-n\mathrm{i}\zeta}) \equiv \omega(\zeta) \quad \text{(B1)}$$

maps the lower half of the ζ-plane to the area below the wavy boundary in the z-plane. In particular, the function maps the θ-axis in the ζ-plane to the wavy boundary in the z-plane, as described by equations (6a) and (b). Before the surface forms any crack, $\omega(\zeta)$ is an analytic function in the lower half of the ζ-plane. When cracks form, the function loses analyticity, namely, $\omega'(\zeta) = 0$ at $\zeta = \pm\pi, \pm 3\pi, \ldots$.

Any plane elastic field can be represented by two analytic functions $\phi(z)$ and $\psi(z)$. Written in terms of the two functions, displacements and resultant forces on the boundary are [29]

$$\frac{E}{1+\nu}\left(u_x+\mathrm{i}u_y\right)=\kappa\phi-z\bar{\phi}'(\bar{z})-\bar{\psi}(\bar{z}) \tag{B2}$$

$$f_x+f_y=-\mathrm{i}[\phi+z\bar{\phi}'(\bar{z})+\bar{\psi}(\bar{z})] \tag{B3}$$

Here E is Young's modulus and ν Poisson's ratio; $\kappa=(3-\nu)/(1+\nu)$ for plane stress and $\kappa=3-4\nu$ for plane strain. The notation $()'$ stands for differentiation of a function with respect to its independent variable.

The two analytic functions are determined by boundary conditions. The imaginary body in Fig. 3 has a simple elastic field corresponding to $\phi=\sigma z/4$ and $\psi=-\sigma z/2$. The body has traction on the wavy boundary, which can be negated by an additional elastic field. Thus, write the complex functions in the current body in Fig. 3 as

$$\phi(z)=\frac{\sigma z}{4}+F(\zeta),\ \psi(z)=-\frac{\sigma z}{2}+Y(\zeta) \tag{B4}$$

where F and Y are the analytic functions representing the additional elastic field. The traction-free condition requires that the resultant force vanish. A combination of equations (B1), (B3) and (B4) gives the boundary condition along the θ-axis on the ζ-plane:

$$\bar{\omega}'(\theta)F(\theta)+\omega(\theta)\bar{F}'(\theta)+\bar{\omega}'(\theta)\bar{Y}(\theta)+\frac{\sigma}{2k}\bar{\omega}'(\theta)[\omega(\theta)-\bar{\omega}(\theta)]=0 \tag{B5}$$

The original elasticity problem now reduces to a problem of finding two functions $F(\zeta)$ and $Y(\zeta)$ that are analytic in the lower half of the ζ-plane, vanish as $\eta\to-\infty$, and satisfy the boundary condition of equation (B5) along the θ-axis.

We solve this boundary value problem by analytic continuation. Collect functions analytic in the upper half plane on one side of the equation, and functions analytic in the lower half plane on the other side of the equation. The theory of function of a complex variable dictates that both sides be a constant in the entire plane.

Evidently the function $\bar{\omega}'(\zeta)\bar{Y}(\zeta)$ is analytic in the upper half plane. Also note that

$$\bar{\omega}'(\zeta)[\omega(\zeta)-\bar{\omega}(\zeta)]=\mathrm{i}\left(1+\alpha_1\mathrm{e}^{\mathrm{i}\zeta}+\ldots+n\alpha_n\mathrm{e}^{n\mathrm{i}\zeta}\right)\left(\alpha_1\mathrm{e}^{-\mathrm{i}\zeta}+\ldots+\alpha_n\mathrm{e}^{-n\mathrm{i}\zeta}+\alpha_1\mathrm{e}^{\mathrm{i}\zeta}+\ldots+\alpha_n\mathrm{e}^{n\mathrm{i}\zeta}\right) \tag{B6}$$

Multiplying term by term, we obtain a sum of terms like $\mathrm{e}^{m\mathrm{i}\zeta}$, which is analytic in the lower half plane for $m<0$, and analytic in the upper half plane for $m>0$. Consequently, the function $\bar{\omega}'(\zeta)[\omega(\zeta)-\bar{\omega}(\zeta)]$ splits into a sum of two parts, one analytic in the upper half plane, and the other analytic in the lower half plane. We make a guess that $F(\zeta)$ takes the form

$$F(\zeta)=-\frac{\mathrm{i}\sigma}{2k}\left(c_1\mathrm{e}^{-\mathrm{i}\zeta}+\ldots+c_n\mathrm{e}^{-n\mathrm{i}\zeta}\right) \tag{B7}$$

The factor in front is so chosen that c values are dimensionless real numbers. We can confirm that equation (B7) is the right form by finding all the coefficients. Split $\bar{\omega}'(\zeta)F(\zeta)$ and $\omega(\zeta)\bar{F}'(\zeta)$ into functions analytic in upper and lower half planes.

In the boundary condition of equation (B5), functions analytic in the lower half plane have terms $\mathrm{e}^{-n\mathrm{i}\theta}$, $\mathrm{e}^{-(n-1)\mathrm{i}\theta}$, …, $\mathrm{e}^{-\mathrm{i}\theta}$. Equating their coefficients term by term, we obtain that

$$\begin{aligned}
&c_n=\alpha_n\\
&c_{n-1}+\alpha_1c_n+\alpha_nc_1=\alpha_{n-1}+\alpha_1\alpha_n\\
&c_{n-2}+\alpha_1c_{n-1}+2\alpha_2c_n+2\alpha_nc_2+\alpha_{n-1}c_1\\
&=\alpha_{n-2}+\alpha_1\alpha_{n-1}+2\alpha_2\alpha_n\\
&\ldots\\
&c_1+\alpha_1c_2+2\alpha_2c_3+\ldots+(n-1)\alpha_{n-1}c_n+\alpha_2c_1\\
&+2\alpha_3c_2+\ldots+(n-1)\alpha_nc_{n-1}\\
&=\alpha_1+\alpha_1\alpha_2+2\alpha_2\alpha_3+\ldots+(n-1)\alpha_{n-1}\alpha_n
\end{aligned} \tag{B8}$$

Once the coefficients of the mapping function, $\alpha_1,\alpha_2,\ldots,\alpha_n$, are prescribed, the above is a set of linear algebraic equations for $c_1,c_2,\ldots,c_n$, which we solve numerically.

The function $Y(\zeta)$ does not take a simple form like equation (B7). Without assuming its form, by equating functions analytic in the upper half plane in equation (B5), we find that

$$Y(\zeta)=\frac{\mathrm{i}\sigma}{2k\omega'(\zeta)}\begin{bmatrix}
\omega'(\zeta)\left(\alpha_1\mathrm{e}^{-\mathrm{i}\zeta}+\ldots+\alpha_n\mathrm{e}^{-n\zeta}\right)-\mathrm{i}\zeta\left(c_1\mathrm{e}^{-\mathrm{i}\zeta}+\ldots+c_n\mathrm{e}^{-n\zeta}\right)\\
-\mathrm{e}^{-0\mathrm{i}\zeta}\left(2\alpha_2c_1+\ldots+2n\alpha_nc_n-\alpha_1^2-\ldots-n\alpha_n^2\right)\\
-\mathrm{e}^{-\mathrm{i}\zeta}\left(2\alpha_2c_1+\ldots+n\alpha_nc_{n-1}+2\alpha_1c_2+\ldots+n\alpha_{n-1}c_n-2\alpha_2\alpha_1-\ldots-n\alpha_n\alpha_{n-1}\right)\\
-\mathrm{e}^{-2\mathrm{i}\zeta}\left(3\alpha_3c_1+\ldots+n\alpha_nc_{n-2}+3\alpha_1c_3+\ldots+n\alpha_{n-2}c_n-3\alpha_3\alpha_1-\ldots-n\alpha_n\alpha_{n-2}\right)\\
\ldots\\
-\mathrm{e}^{-(n-1)\mathrm{i}\zeta}n\left(\alpha_1c_n+\alpha_nc_1-\alpha_1\alpha_n\right)
\end{bmatrix} \tag{B9}$$

On the surface of the current body, because the resultant force vanishes, a combination of equations (B2) and (B3) shows that the elastic displacements on the surface are given by

$$u_x+\mathrm{i}u_y=\frac{4\phi}{E} \tag{B10}$$

The above result is valid under the plane stress conditions; replace E by $E/(1-\nu^2)$ under the plane strain conditions.

APPENDIX C

Determination of the generalized forces

A component of the generalized force is

$$f_\mathrm{p}=-\frac{\partial U_\mathrm{S}}{\partial\alpha_\mathrm{p}}-\frac{\partial U_\mathrm{B}}{\partial\alpha_\mathrm{p}}-\frac{\partial U_\mathrm{C}}{\partial\alpha_\mathrm{p}}-\frac{\partial U_\mathrm{E}}{\partial\alpha_\mathrm{p}} \tag{C1}$$

where

$$\frac{\partial U_\mathrm{S}}{\partial\alpha_\mathrm{p}}=\gamma_\mathrm{S}\int\frac{p\cos p\theta-p\sin p\theta}{k\partial s/\partial\theta}$$

$$\frac{\partial U_\mathrm{B}}{\partial\alpha_\mathrm{p}}=(-1)\,p\frac{\gamma_\mathrm{B}}{k}$$

$$\frac{\partial U_\mathrm{C}}{\partial\alpha_\mathrm{p}}=\frac{\pi g}{k^2}\begin{cases}2 & p=0\\ 2p\alpha_p & p\neq0\end{cases}$$

$$\frac{\partial U_\mathrm{E}}{\partial\alpha_\mathrm{p}}=\begin{cases}0 & p=0\\ \dfrac{\pi\sigma^2}{k^2E}\left[p\alpha_p-pc_p-\displaystyle\sum_{q=1}^{n}q\alpha_q\frac{\partial c_q}{\partial\alpha_p}\right] & p\geq1\end{cases} \tag{C2}$$

Let $\mathbf{a}=(\alpha_1\ \alpha_2\ \ldots\ \alpha_n)^\mathrm{T}$ and $\mathbf{c}=(c_1\ c_2\ \ldots\ c_n)^\mathrm{T}$. To calculate the last two terms in equation (C2), we need to solve

c and the derivative of **c** with respect to **a**. Equation (B8) can be written as

$$\left(\mathbf{A}^{(1)}+\mathbf{A}^{(2)}\right)\mathbf{c}=\mathbf{A}^{(1)}\mathbf{a} \tag{C3}$$

where $\mathbf{A}^{(1)}$ and $\mathbf{A}^{(2)}$ are n by n matrices with elements

$$A_{ij}^{(1)}=\begin{cases}0 & i>j\\ 1 & i=j\\ (j-i)\alpha_{j-i} & i<j\end{cases}$$

$$A_{ij}^{(2)}=\begin{cases}0 & j>n-i\\ j\alpha_{j+i} & j\le n-i\end{cases}$$

Let $\mathbf{A}=\mathbf{A}^{(1)}+\mathbf{A}^{(2)}$. We obtain **c** by solving equation (C3),

$$\mathbf{c}=\mathbf{A}^{-1}\mathbf{A}^{(1)}\boldsymbol{a} \tag{C4}$$

equation (B8) can also be written as

$$\left(\mathbf{C}^{(1)}+\mathbf{C}^{(2)}\right)\mathbf{a}+\mathbf{c}=\mathbf{A}^{(1)}\mathbf{a} \tag{C5}$$

where $\mathbf{C}^{(1)}$ and $\mathbf{C}^{(2)}$ are n by n matrices with elements

$$C_{ij}^{(1)}=\begin{cases}0 & j>n-i\\ jc_{j+i} & j\le n-i\end{cases}$$

$$C_{ij}^{(2)}=\begin{cases}0 & j\le i\\ (j-i)c_{j-i} & j>i\end{cases}$$

Let $\mathbf{C}=\mathbf{C}^{(1)}+\mathbf{C}^{(2)}$. A differentiation of both sides of equation (B8) gives

$$\mathbf{A}\mathrm{d}\mathbf{c}+\mathbf{C}\mathrm{d}\mathbf{a}=\left(\mathrm{d}\mathbf{A}^{(1)}\right)\mathbf{a}+\mathbf{A}^{(1)}\mathrm{d}\mathbf{a} \tag{C6}$$

With $(\mathrm{d}\mathbf{A}^{(1)})\mathbf{a}$, we find that

$$\left(\mathrm{d}\mathbf{A}^{(1)}\right)\mathbf{a}=\mathbf{A}^{(2)}\mathrm{d}\mathbf{a} \tag{C7}$$

A substitution of equation (C7) into equation (C6), gives

$$\mathrm{d}\mathbf{c}=\mathbf{A}^{-1}(\mathbf{A}-\mathbf{C})\mathrm{d}\mathbf{a} \tag{C8}$$